JOM
https://doi.org/10.1007/s11837-023-05852-0

Multiscale Effects of Collagen Damage in Cortical Bone and Dentin

QIAN WU,[1,5] SHANGAYA TOURAIVANE,[1,6] THOMAS REISS,[1,7] MAXIME VALLET,[1,2,8] NICOLAS ROUBIER,[1,9] ELSA VENNAT,[1,10] and CLAIRE ACEVEDO [3,4,11]

1.—LMPS, Université Paris-Saclay, CentraleSupélec, ENS Paris-Saclay, CNRS, LMPS - Laboratoire de Mécanique Paris-Saclay, 3 Rue Joliot Curie, 91190 Gif-sur-Yvette, France. 2.—Université Paris-Saclay, CentraleSupélec, ENS Paris-Saclay, CNRS, Laboratoire SPMS, 3 Rue Joliot Curie, 91190 Gif-sur-Yvette, France. 3.—Department of Mechanical Engineering, University of Utah, Salt Lake City, UT 84112, USA. 4.—Department of Biomedical Engineering, University of Utah, Salt Lake City, UT 84112, USA. 5.—e-mail: qian.wu.w@outlook.com. 6.—e-mail: shangaya.touraivane@ens-paris-saclay.fr. 7.—e-mail: thomas.reiss@centralesupelec.fr. 8.—e-mail: maxime.vallet@centralesupelec.fr. 9.—e-mail: nicolas.roubier@centralesupelec.fr. 10.—e-mail: elsa.vennat@centralesupelec.fr. 11.—e-mail: claire.acevedo@utah.edu

The denaturation of collagen at the molecular level in bone and dentin can impact their structure and properties, leading to increased brittleness in pathological diseases such as osteogenesis imperfecta, dentinogenesis imperfecta, diabetes, and cancer. This study investigates the relationship between collagen denaturation and the macroscale resistance of bone and dentin. Through heat treatment at 160°C on bovine bone and human dentin, the effects of collagen denaturation on macroscale flexural strength, scanning electron microscopy, and transmission electron microscopy imaging of micro- and nanostructure were studied. The results show that collagen denaturation decreases the resistance of bone and dentin to fracture, even though collagen denaturation did not impact the mineral organization around and inside collagen fibrils. This is attributable to (1) a reduction in bone and dentin ability to deform (e.g., 40–75% decrease in strain to failure) and to resist fracture (e.g., 83–95% decrease in work to fracture) properties and (2) to a smoother crack path with less crack deflection around microstructural features. Reduction in deformation and toughness not only removed plastic deformation but also drastically decreased elastic deformation and elastic work to fracture in all tissues. However, the elastic modulus was only affected in radial-oriented bone samples where collagen fibrils are oriented perpendicularly to crack opening forces. This study highlights the crucial role of collagen molecule integrity and orientation in bone/dentin deformability and resistance.

INTRODUCTION

Mineralized tissues such as bone and dentin exhibit unique mechanical properties and resistance to fracture, which are imparted by their hierarchical structure ranging from nanoscale to macroscale.[1,2] However, in patients with genetic disorders like osteogenesis imperfecta (OI) and dentinogenesis imperfecta type 1 (OIDI)[3–5] or fragility diseases related to diabetes or cancer,[6–8] these tissues become weaker and more prone to fracture. The aim of this study is to isolate the factors and pertinent length scale associated with the loss of plasticity and toughness that contribute to the brittleness of bone and dentin in these patients, with the hope of finding new therapeutic targets to reduce the risk of fracture.

(Received February 6, 2023; accepted April 10, 2023)

Published online: 19 May 2023

The complex hierarchical structure of bone and dentin is at the origin of their unique stiffness (i.e., ability to resist elastic deformation), strength (i.e., ability to resist plastic deformation), and toughness (i.e., ability to resist fracture) properties; however, different properties originate at widely differing structural length scales.[9] Regarding fracture resistance, the ductility in bone or dentin results from "plasticity" mechanisms that principally operate at sub-micron (10 to 100 nm) scales via such processes as the sliding of mineralized collagen fibrils;[10,11] this contributes to the intrinsic toughness of bone. Extrinsic toughness, conversely, is generated at much coarser length scales (1 to 100 s mm) via the nature of the crack path and its effect of "shielding" the crack via such mechanisms as crack bridging and deflection.[9,12] These widely divergent length-scale mechanisms are coupled, however.[13] When "plasticity" (intrinsic toughness) in bone or dentin is curtailed because of restricted collagen fibrillar sliding, as can occur in diabetes from excessive collagen cross-linking, or in OI/DI due to type I collagen mutation, the tissue dissipates energy at higher length scales by microcracking; the microcracking, in turn, promotes extrinsic toughening by motivating the formation of uncracked ligament[14] and crack deflection.

At the nanoscale (collagen-mineral level), the collagenous mineralized matrix of bone and dentin have similar characteristics in composition (approximately 70% weight of hydroxyapatite crystals, 20% of collagen, and 10% of water[15,16]). At the microscale, cortical bone is made up of concentric lamellae forming osteons around the central Haversian canals, which contain the bone's blood vessels, nerves, and lymphatic vessels.[9,17,18] The orientation of osteons in the longitudinal direction forms the Haversian systems. Each osteonal lamella comprises mineralized collagen fibers, consisting of collagen fibrils, formed of collagen molecules, all mainly arranged in the longitudinal direction of the bone.[19,20] The interstitial spaces between the lamellae (about 4 μm depth, 10 μm width, and 17 μm length[21,22]) house the osteocyte cells, which play a critical role in bone remodeling through their dendritic branches (i.e., canaliculi with an average diameter of about 100–600 nm[21,22]) that communicate with other cells and remodel the local bone matrix.[23] At the microscale, crown dentin is made up of tubules (1 μm diameter) extending radially from the pulp towards the dentin-enamel junction,[24] with small lateral branches (0.2 μm diameter) extending peripherally from the tubules.[25] The collagen fibrils in the dentin are isotropically distributed in the plane perpendicular to the tubule axis.[26]

Disruption of the nanostructure or microstructure in mineralized tissues causes bone fragility by impairing intrinsic or extrinsic toughness mechanisms. Diseases and genetic disorders can also impact the cells involved in repairing and maintaining tissue matrix composition, organization, and function. The healing processes in bone and dentin differ,[27] with bone being regenerative (i.e., the tissue is remodeled similarly to the original structure) while dentin is reparative (i.e., nonsimilar morphological features).[27] Phylogenetic studies have shown that dentin analogs were initially similar to bone,[28–30] but during evolution, the odontoblast-like cells in dentin were located within alveoli, as is the case for osteocytes surrounded by bone within lacunae. During evolution, the cell bodies in dentin were then located outside the mineralized tissue (contrary to bone tissues), along the border of the mineralization front, and their long branches occupied the lumen of dentin tubules.[28–30] Vascularization also evolved differently between both tissues, displaying a dense network of blood vessels supplying nutrients in bone whereas dentin is not vascularized.[30] These two different healing processes will affect the anisotropy and porosity of the tissue structures, the mechanical properties, and the repair of microcracks which are involved in intrinsic and extrinsic toughness mechanisms.

Because dentin and bone are mineralized tissues with similar genetic origins, genetic disorders and diseases result in fragility in both types of tissues.[31] This is the case of osteogenesis imperfecta and dentinogenesis imperfecta type 1, both caused by a mutation of the genes encoding type I collagen, which results in loss of tissue resistance to fracture.[4] Type I collagen defects in diabetes,[6,7] cancer,[8] and age[32,33] also significantly deteriorate mechanical properties by cross-linking and stiffening the collagen in bone and teeth. This highlights the critical role collagen plays in bone and dentin strength and resistance to fracture despite their different multiscale structures. However, because genetic disorders and diseases in bone and dentin affect different factors of tissue quality spanning from the nano- to macroscale (e.g., composition, structure, properties, cell-mediated remodeling/regeneration), it is difficult to evaluate the sole contribution of collagen damage. Therefore, the origins of the brittleness affecting bone and dentin in genetic and fragility diseases are poorly understood. This knowledge would help evaluate the fracture risk and identify new collagen targets for future treatment development. Our hypothesis is that collagen molecular denaturation will alter mechanical resistance at the macroscale and affect fracture mechanisms at the microscale and nanoscale. To test this hypothesis, we used a heat-treatment model on human dentin and bovine cortical bone known to induce 10% collagen damage[13] after 2 h at 160°C[34] in a similar way to collagen molecular unfolding associated with pathological conditions.[35] We quantified tissue mechanical properties using flexural strength tests. We visualized tissue structures at the micro- and nanoscales and compared the fractured surface

using scanning electron microscopy (SEM) and transmission electron microscopy (TEM). The heat-treatment model allows us to modify the collagen molecules and isolate differences in structure and tissue mechanical properties within bone and dentin.

MATERIALS AND METHODS

Samples and Preparation

Bone samples were obtained from the tibial mid-diaphysis tibia of a young adult (2–3 year-old) bovine and dentin samples from two non-carious human third molars of a 23-year-old donor. Bone samples were extracted from the anterior quadrant (compression side), which has been shown to be dominated by osteon microstructure with a limited plexiform bone.[36,37] The bone specimens are collected from areas that are relatively close to each other, with a maximum distance of 3 cm between them. Since the dentin area of a tooth is small (only a few millimeters in distance), the dentin specimens are obtained from regions even closer to each other than the bone specimens. The samples were fixed during sectioning using a cutter disc to ensure parallelism. The disc cut the first surface before moving sideways to cut the following surfaces. Bone and dentin samples were sectioned using a low-speed diamond saw (Struers Secotom-10 and Buehler) and then ground and polished under constant irrigation down to beam dimensions of 1 mm thickness, 1 mm width, and 10 mm length. Finally, the dimensions were measured at different positions to verify parallelism. Bone samples were cut in two different directions: along the direction of Haversian canals for longitudinal-oriented samples and perpendicular to the direction of Haversian canals for radial-oriented samples (Fig. 1). Dentin samples were cut in the radial direction for radial-oriented samples (Fig. 1). Each type of sample was separated into two groups: a heat-treated group and an untreated control group. The samples are named D for control dentin, DH for heat-treated dentin, L for control longitudinal bone, LH for heat-treated longitudinal-oriented bone, R for control radial bone, and RH for heat-treated radial-oriented bone. Six samples were taken for each configuration. To avoid the impact of sample dehydration on the experiemental results, the samples were stored in Ringer's solution at 4 °C for at least 24 h prior to mechanical testing.

Flexural Strength Tests

Bone and dentin mechanical properties were measured using flexural strength tests of beam-shaped samples in three-point bending (N = 6 / group) in general accordance with ASTM D790. Flexural tests were carried out using a SHIMADZU AGS-X stage with 500 N load cell under displacement control with a displacement rate of 0.05 mm/min. Force and displacement data were recorded every 0.01 s and used to calculate stress and strain using beam theory. Mechanical properties (bending stiffness, yield stress, yield strain, ultimate stress, strain to failure, work to fracture) were then evaluated from the stress–strain plots.

Scanning Electron Microscopy Imaging and Fractography

To explore the microstructure of cortical bone and dentin, we observed the fractured surfaces of mechanically tested samples (N = 6 /group) using LEO Gemini 1530 (Zeiss) scanning electron microscopy (SEM) equipped with a Schottky field emission gun (FEG). The SEM was operated at electron beam accelerating voltage of 3 kV. The samples were coated by a layer of silver on side surfaces and a fine layer of carbon (transparent to electron beam but conductive) on the observed surface to enable and improve the imaging.

Section Preparation with Dual-Focused Ion Beam-Scanning Electron Microscopy (FIB-SEM)

Sections for transmission electron microscopy (TEM) imaging were obtained at the fracture surface of mechanically tested samples using FIB-SEM lift-out procedures. We used a Helios Nanolab 660 FIB-SEM equipped with an ion gun, platinum gas injector system, and micro-manipulator. To reduce charging, the samples were held on a metal support and solidified by silver lacquer and covered by fine carbon layers. For longitudinal bone samples, lamina cuts were extracted in the radial direction of an osteon between two osteonal lamellae with collagen fibril and fibers oriented in the section plane (Fig. 2a). For radial bone, lamina cuts were extracted inside an osteonal lamella and parallel to the direction of the Haversian canal. For dentin, laminae were extracted between two tubules and in the direction parallel to them so that fibril and fibers are oriented in the section plane (Fig. 2b).

Transmission Electron Microscopy Observation

To image and analyze bone and dentin at a nanometric scale, we employed TEM. For TEM observation, one representative fractured sample from each group was chosen based on its bending modulus, yield stress and strain, and ultimate stress and strain to failure. The imaging was conducted using a Titan3 G2 80-300 TEM. Collagen fibril-mineral crystal level samples were imaged using bright-field (BF) TEM imaging, while selected area electron diffraction (SAED) was used to determine the crystal orientation.

For each lamina, the TEM bright-field images taken at different locations were assembled. Reconstruction was carried out using photo stitching (ImageJ software).

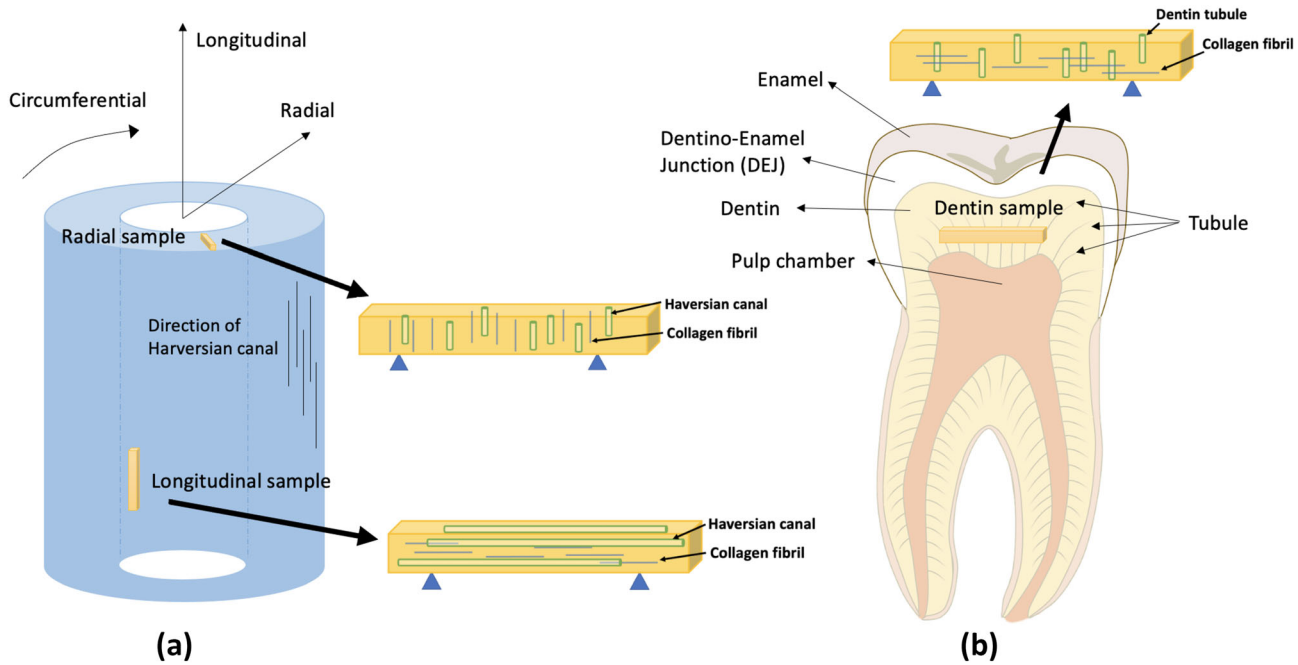

Fig. 1. Orientation of the longitudinal and radial samples in (**a**) bone cortex and (**b**) dentin area.

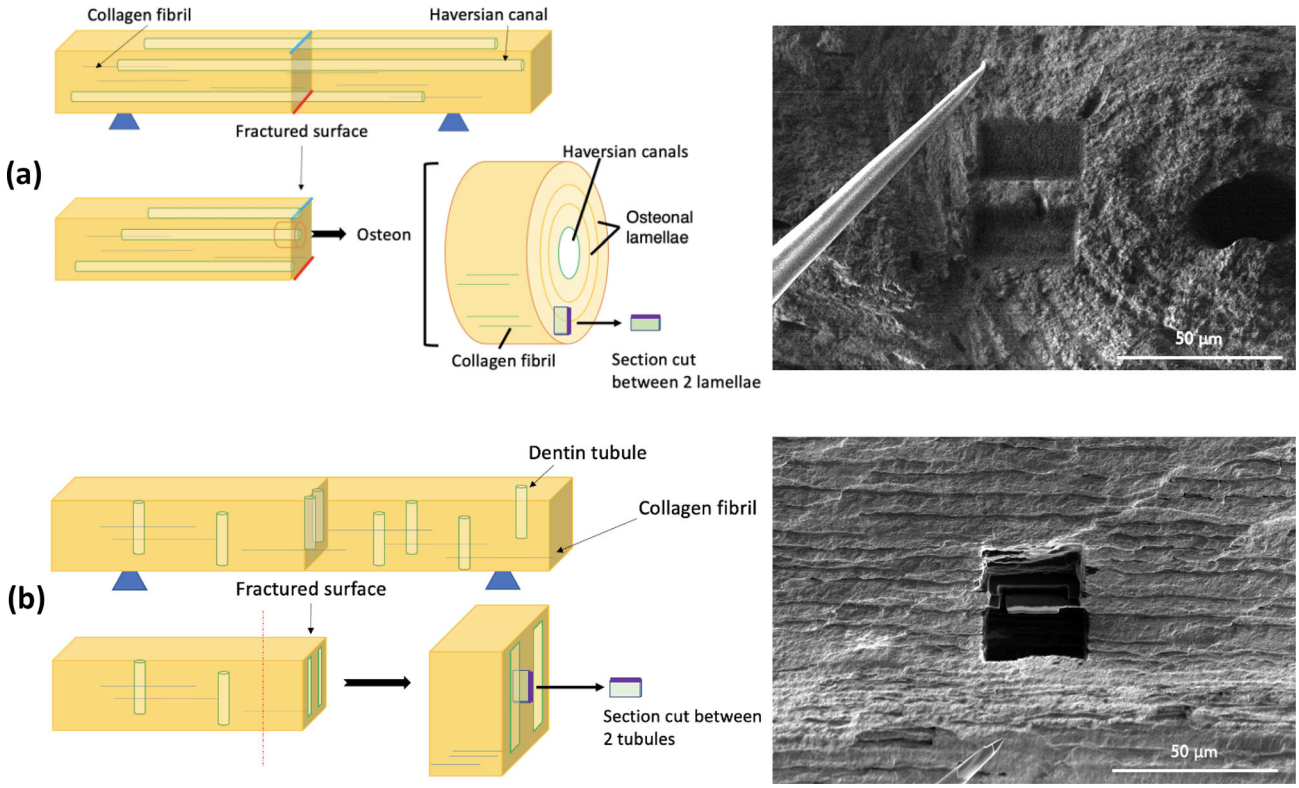

Fig. 2. (**a**) For longitudinal bone, the section was extracted in the radial direction of an osteon between two osteonal lamellae with collagen fibril and fibers oriented in the section plane. (**b**) For dentin, the section was extracted between two tubules and in the direction parallel to them so that fibril and fibers are oriented in the section plane.

Statistics

Stress–strain data were compared between control (untreated) and treated samples from a specific tissue (bone or dentin) using Mann-Whitney test. Statistical tests were performed with R project. Significance was defined by $p < 0.05$. All data are given as mean ± standard error.

RESULTS

Collagen Denaturation Significantly Impacts the Mechanical Properties of Both Dentin and Bone

We evaluated the mechanical properties of cortical bone samples and dentin samples using three-point bending tests. Both bone and dentin mechanical properties have been significantly affected by collagen denaturation induced by heat treatment. We observed a decrease in strength and work to fracture for all the heat-treated samples as well as varying trends in the evolution of their elastic moduli. Longitudinally oriented bone samples (N = 6 in L group and 6 in LH group, Table I, Fig. 3a) showed a drastic and significant loss of post-yield properties with 70% decrease ($p< 0.01$) in strain to failure and 92% decrease ($p<0.01$) in work to fracture in samples with heat-induced collagen damage. However, elastic moduli were not significantly affected by heat treatment (Fig. 3a).

Radially oriented bone samples (N = 6 in R group and RH group, Fig. 3b) also show a dramatic drop in strain to failure (39% decrease, $p < 0.01$) and work to fracture (83% decrease, $p < 0.01$) with heat treatment, this time associated with a significant decrease in elastic properties such as bending modulus and yield stress ($p < 0.05$). Dentin mechanical behavior (N = 6 samples in D group and in DH group, Fig. 3c) reveals similar changes in strain to failure (75% decrease, $p = 0.04$) and work to fracture (95% decrease, $p = 0.04$) than in longitudinal bone samples (70% decrease, $p < 0.01$ in strain to failure and 92% decrease, $p < 0.01$ in work to fracture) without change in bending modulus. However, dentin mechanical behavior does not display plastic deformation. Comparison between tissues indicates that the ultimate stress of the untreated radial-oriented bone is four times lower ($p = 0.02$) than that of the untreated longitudinal-oriented bone and 2.8 times lower ($p < 0.01$) than that of the dentin. The elastic stress-strain behavior of dentin is identical to that of longitudinal bone, but it lacks the ability to undergo plastic deformation.

Fracture Surface and Structure Imaging at Micrometer Scales

Fracture surfaces obtained from the flexural test were observed using scanning electron microscopy (SEM). In longitudinal-oriented bone, the fracture surface of the heat-treated sample LH (Fig. 4c) is seen to be scaly with many small flat areas and clear steps in the crack path whereas the fracture surface is rougher in the control sample L with no steps to be seen (Fig. 4a). The side view of samples (Fig. 4b) reveals crack deflection indicated by changes in crack angles along the crack path in the L samples, whereas in the LH samples, the crack propagates in a flat manner (or smoothly curved) with no tortuosity in between an abrupt jump of the crack (Fig. 4d) (indicated by 90°change in crack angle). Roughness and abrupt changes in crack direction are almost nonexistent in radial samples. The crack propagates in a really straight manner with a fairly smooth crack surface in both heat-treated RH and control R samples (Fig. 4e–h). In dentin samples, we observed a smoother fracture surface in the heat-treated sample DH (Fig. 4k) compared to the control sample D (Fig. 4i). We also noticed a curved shape in the crack path that was intermittently interrupted by a change in crack direction (indicated by the write arrow in Fig. 4i) when the crack crossed the neutral axis (transition between tension and compression areas) (Fig. 4j). Less crack deflection was observed at the neutral axis in the heat-treated dentin sample DH (Fig. 4l).

Structure Characterization at the Nanometer Scale

From the bright-field TEM images, we do not find significant visual differences between the untreated and heat-treated sample (Fig. 5). The collagen fibrils in L (or LH) are lying within the TEM section plane whereas for D and DH samples collagen fibrils are crossing the plane of the TEM section in accordance with the knowledge of the collagen fibril organization in bone and dentin.[26,38]

We found that in areas relatively far from pores or voids such as lacunae and canaliculi, the collagen fibrils are roughly organized in one direction. Correspondingly, in these “ordered” areas, the electron diffraction patterns show preferred orientations (Supplementary Fig. 1). In areas near canaliculus or near a lacuna, collagen fibrils are arranged in different directions, crossed and overlapped. In these areas, the diffraction spots are distributed at different angles and nearly form a ring (Supplementary Fig. 1). On the other hand, in the TEM image of longitudinal control bone, we observed that the collagen fibrils were arranged in a “chaotic” manner at the interface between two adjacent osteon lamellae, with a sudden change in the direction of the collagen fibrils (Supplementary Fig. 2), as described by Wagermaier et al.[39] The TEM bright-field imaging was also used to measure the periodicity of the banding pattern along collagen fibrils because of the periodic arrangement of mineral crystals. We found an average periodicity of 63.6 nm for the control bone (with standard deviation 2.8 nm) and 63.8 nm for heat-treated bone (standard deviation 2.8 nm). The heat treatment does not significantly change the average periodicity of collagen banding and its variability. High-resolution TEM imaging was used to observe the interatomic distance along the c-axis of hydroxyapatite crystals (Supplementary Fig. 3). As a result, the average interatomic distance is 0.341 nm for the control bone (N = 5) and 0.344 nm for the heat-treated bone (N = 2).

Table I. Mechanical properties in bovine cortical bone and human dentine measured on hydrated samples (untreated or heat treated) using flexural strength tests

	Bone (Longit.)		
	L	**LH**	**% change**
Bending modulus (GPa)	8.9 ± 1.7	7.2 ± 0.8	19%
Yield stress (MPa)	276.0 ± 38.8	93.3 ± 8.3 **	66%
Ultimate stress (MPa)	314.5 ± 36.2	93.3 ± 8.3 **	70%
Yield strain (%)	3.4 ± 0.9	1.4 ± 0.2 **	59%
Strain to failure (%)	4.6 ± 0.4	1.4 ± 0.2 **	70%
Work to fracture W_f (J/m^2)	2.4 ± 0.3	0.19 ± 0.34 **	92%
Preyield W_f (J/m^2)	1.4 ± 0.4	0.17 ± 0.03 **	88%
Postyield W_f (J/m^2)			
0.9 ± 0.40.03 ± 0.02 **97%			
		Bone (Radial)	
	R	RH	% change
Bending modulus (GPa)	5.2 ± 0.8	2.8 ± 1.1 **	46%
Yield stress (MPa)	63.2 ± 4.3	16.0 ± 6.2 *	75%
Ultimate stress (MPa)	75.9 ± 11.6	20.4 ± 7.6 **	73%
Yield strain (%)	1.55 ± 0.03	0.9 ± 0.1 *	42%
Strain to failure (%)	1.65 ± 0.2	1.0 ± 0.2 **	39%
Work to fracture W_f (J/m^2)	0.19 ± 0.02	0.03 ± 0.01 **	83%
Preyield W_f (J/m^2)	0.11 ± 0.05	0.01 ± 0.01 **	91%
Postyield W_f (J/m^2)	0.08 ± 0.05	0.02 ± 0.01	75%
		Dentin	
	D	DH	% change
Bending modulus (GPa)	8.6 ± 1.2	7.0 ± 1.7	19%
Yield stress (MPa)	223.5 ± 29.9	44.1 ± 35.2 *	81%
Ultimate stress (MPa)	212.0 ± 59.1	44.1 ± 35.2 *	79%
Yield strain (%)	2.6 ± 0.1	0.7 ± 0.4 *	73%
Strain to failure (%)	2.7 ± 0.5	0.7 ± 0.4 *	75%
Work to fracture W_f (J/m^2)	0.9 ± 0.4	0.04 ± 0.09 *	95%
Preyield W_f (J/m^2)	0.7 ± 0.3	0.04 ± 0.09 *	95%
Postyield W_f (J/m^2)	0.2 ± 0.1	0.01 ± 0.00 *	96%

H stands for "heat-treated". Values marked with ** are such that $p<0.01$, values marked with * are such that $p<0.05$ and values not marked did not reach $p=0.05$.

DISCUSSION

Our results show that collagen denaturation at the molecular scale impacts mineralized tissue behavior and resistance in bovine bone and human dentin. We found that the loss of fracture resistance is due to a significant decrease in the tissue's ability to deform (plastically and elastically) independently of the collagen fibrillar orientation and independently of the type of tissue. More specifically, 70–75% loss of strain to failure in longitudinal bone and dentin and 39% in radial bone ($p < 0.05$) was associated with 80–95% decrease ($p < 0.05$) in fracture resistance (i.e., work to fracture) of bone and dentin compared with control samples. This loss of resistance and deformation capacity coincided with a smoothing of the fracture crack surface in heat-treated longitudinal bone and dentin samples where collagen fibrils cross the crack plane. In the radial-oriented bone samples, where collagen fibrils were oriented in the plane of the crack, the crack plane was flat without visible differences between groups. The flexural strength response of dentin and longitudinal-oriented bone samples overlaps almost perfectly in the linear elastic region, though bone material also presents a post-yield behavior indicative that bone is less prone to brittle rupture than dentin. The observed low plasticity of dentin is consistent with the study of Ryou et al.[40] In agreement with previous studies, we observed that collagen damage significantly reduces macroscale toughness and post-yield properties, and a

compromised collagen network has reduced amounts of crack deflection.[13] Our new data show that collagen denaturation by heating has a similar impact on mechanical properties and on the fracture crack surface for longitudinal-oriented bone and dentine, different from radial-oriented bone. Our TEM imaging did not indicate any differences in the nanoscale organization and structure of collagen fibrils and minerals with heat treatment. These findings show that collagen molecule integrity is key to maintaining the ability of bone and dentin to deform and dissipate large amounts of energy via collagen fibril mechanisms inducing crack roughness. Collagen denaturation at the molecular level impairs bone and dentin properties without changing the nano- and microstructure of these tissues.

Heat Treatment Does Not Affect the Structure of Mineralized Collagen Fibrils at the Nanoscale

In this study, we used heat denaturation as a model to induce a local triple helix unfolding. We have shown in previous studies[13] that the heat treatment model of bovine cortical bone at 160 °C for 2 h denatures approximately 10% of collagen molecules, which affect bone macroscale properties in a similar way as fragility diseases.[6,34,35,41–47] We did not find a change in fibril direction or local damage along collagen fibrils at the nanoscale using TEM imaging. These two aspects are known to have a determinant effect on bone and dentin strength.[48,49] This result is consistent with the literature[50] indicating that the orientation of aligned collagen is unchanged with heating. Even though the nanostructure was not visually affected, breaking of collagen enzymatic and non-enzymatic cross-links or H-bonds can occur during heat denaturation,[51–53] which would lead to a less stabilized or even fragmented collagen fibril and molecules. This kind of effect would impact the collagen banding periodicity[54] (known to be approximately 67 nm for healthy bone[55,56]) or at least its variability. Neither the average periodicity of collagen banding nor its variability was altered by the heat denaturation in dehydrated samples (63.6 ± 2.8 nm in untreated versus 63.8 ± 2.8 nm in untreated samples). The AFM technique may help to further investigate the collagen. In bones with osteogenesis imperfecta, Formino et al.[57] and Stylianou et al.[58] found that although the average spacing remains unchanged, it presents more significant variability than healthy bones. Unlike OI bone, which combines several mechanisms of collagen alteration, the mechanism of collagen denaturation induced by heat treatment is primarily due to unfolding triple helix structures in collagen molecules. The heat treatment does not affect the crystal nanostructure either: the interatomic distance along the c-axis of hydroxyapatite crystals is unchanged.[59] The values for the control and heat-treated samples are approximately 0.34 nm, as in other studies.[60,61] Our study did not bring evidence of a significant impact of heating on the nanoscale level of bone and dentin tissues. The loss of tissue material properties was a direct effect of collagen molecular denaturation as indicated in our previous study.[13] In this study, a similar heat treatment in bone caused a two to three time reduction in crack initiation toughness, an intrinsic toughness mechanism known to be associated with collagen-induced plasticity.[62]

Collagen Denaturation Alters Crack Propagation at the Microstructural Level

The crack propagation path at the micrometer scale is characterized by less tortuosity and a less rough fracture surface in treated bones leading to fewer crack deflections (e.g., fewer changes in angles). Since crack deflection is the main extrinsic toughening mechanism in bone using the weakest microstructural resistance (along the cement lines parallel to the long axis of the bone),[14,63,64] the smoothing of the crack surface in longitudinal-oriented bones indicates that less energy is necessary to propagate a crack through in denatured samples. One explanation is that denatured collagen can create a “weaker path” than the cement line for the crack to propagate. These results are consistent with[13] where denatured collagen in bovine cortical bone was associated with three times fewer crack deflections and a 15°reduction in crack deflection angle. In dentin, the crack surface in treated samples is also smoother. When we compare longitudinal bone and dentin microstructure, the crack is perpendicular to the orientation of the fibril plane (where fibrils are isotropically distributed) but follows the tubule orientation in dentin (whereas the crack cuts the osteons in bone).[26] This was shown to be the toughest direction with a 50% higher work of fracture in the plane perpendicular to collagen fibrils (parallel to the tubules).[65–67] There is a possibility that denatured collagen increases the common occurrence of microcracks in the peritubular dentin surrounding the tubules,[12] which would allow the crack to propagate with less energy.

In radial-oriented bone, this smoothing effect with collagen denaturation is not distinguished on the flat crack surface of both treated and untreated samples. The flat and straight crack path is due to the fact that the direction of the paths of maximum driving force coincides with the weakest microstructural resistance (along the cement lines).[9] It is difficult to compare how the collagen denaturation weakening competes with cement line weakness since both lead a low-energy crack parallel to their direction. Denaturation of collagen has a stronger impact on longitudinal-oriented bone and dentin by weakening the cutting resistance of collagen fibrils

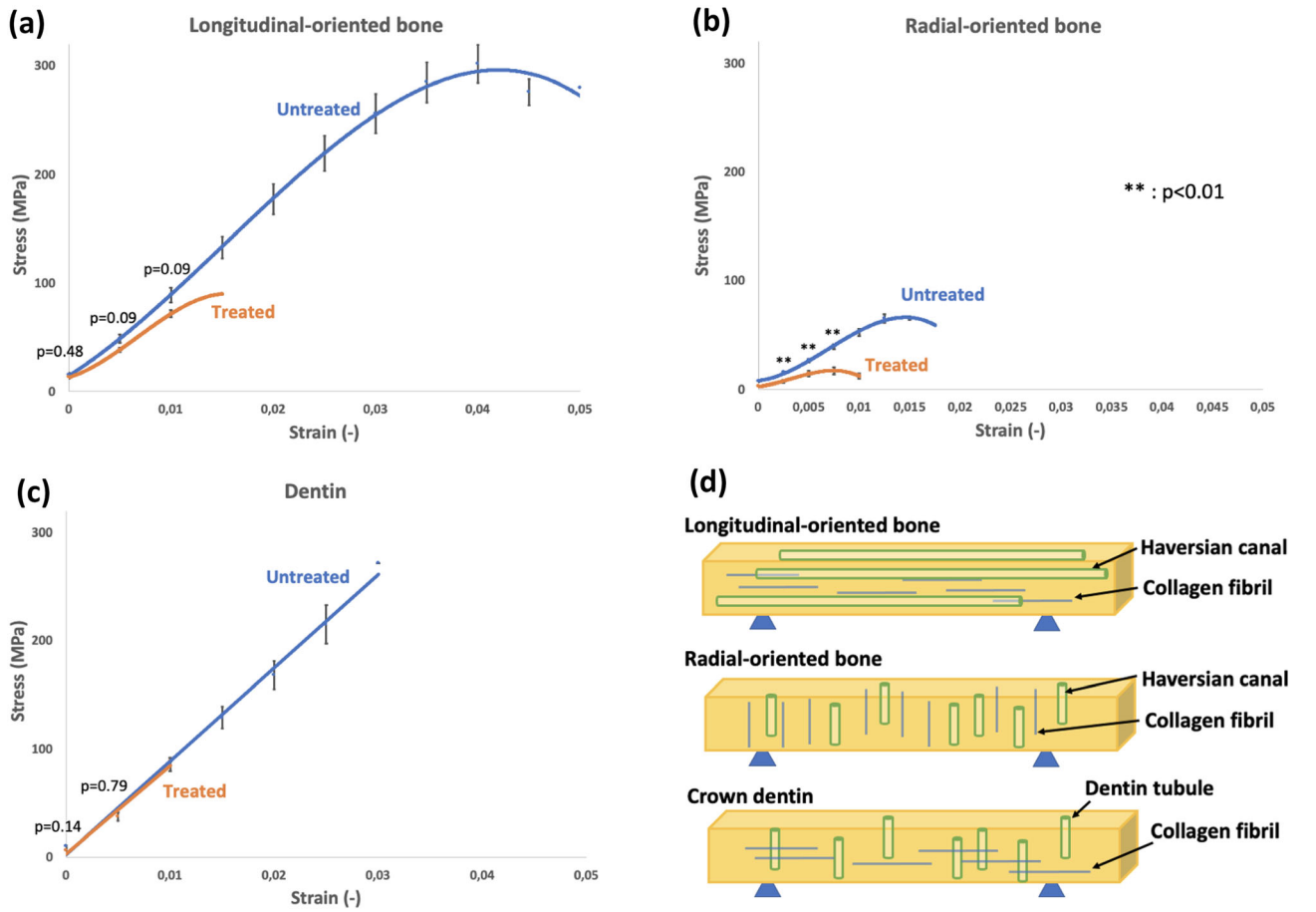

Fig. 3. Mechanical properties of (**a**) bovine longitudinal-oriented cortical bone, (**b**) bovine radial-oriented cortical bone, and (**c**) human dentin, comparing the heat-treated groups and untreated (control) groups. For each individual flexural test, the strain values are binned every 0.5% strain for longitudinal-oriented bone and dentin and every 0.25% strain for radial-oriented bone. Then, for each group, the average and standard error of the binned values are calculated and shown as the trendline and error bars, respectively. Finally, *p*-values of the binned values are calculated to compare the heat-treated group and the untreated group for statistical differences. (**d**) Orientation of Haversian canals and collagen fibrils in cortical bone samples as well as the orientation of tubules and collagen fibrils in dentin samples.

whereas in radial-oriented bone the propagation along the cement lines seems to already be a low-energy dissipation mechanism.

Collagen Denaturation Induces Bone and Dentin Fragility at the Macroscopic Scale

Collagen denaturation creates bone fragility in bone and dentin, which is related to loss of mechanical properties at higher length scales.

Bending modulus in longitudinal-oriented bone and dentin samples (Fig. 3A and C) is not affected by the collagen denaturation induced by heat treatment because the elastic modulus of bone is mostly affected by minerals,[68–70] which are not degraded under heat treatment at 160°C. However, the bending modulus decreases after heat treatment for radial-oriented bone. One explanation would be to consider the tissue as a composite of collagen fibrils and hydroxyapatite crystals as explained hereafter.

Radial bone can be modeled in a very simplistic way with a Reuss configuration[71] where the Young's modulus of the composite E_R can be assessed by:

$$E_R = \frac{1}{\frac{c_f}{E_f} + \frac{c_{HAP}}{E_{HAP}}} \quad (1)$$

with c_f the volume of collagen fibrils, c_{HAP} the volume of hydroxyapatite crystals, E_f the, E_f/E_{HAP} the Young's modulus of the fibrils, E_{HAP} the Young's modulus of hydroxyapatite crystals, and E_R the composite (tissue) Young's modulus. This equation indicates that when the fibrils Young's modulus E_f decreases, the composite Young's modulus will decrease. The similar direction of collagen fibrils and mineralized cement lines along the osteons might be why both mineral and collagen moduli play an essential role in the whole-material stiffness. The E_f decrease can be due to the denaturation of collagen or to a microcracked interface with

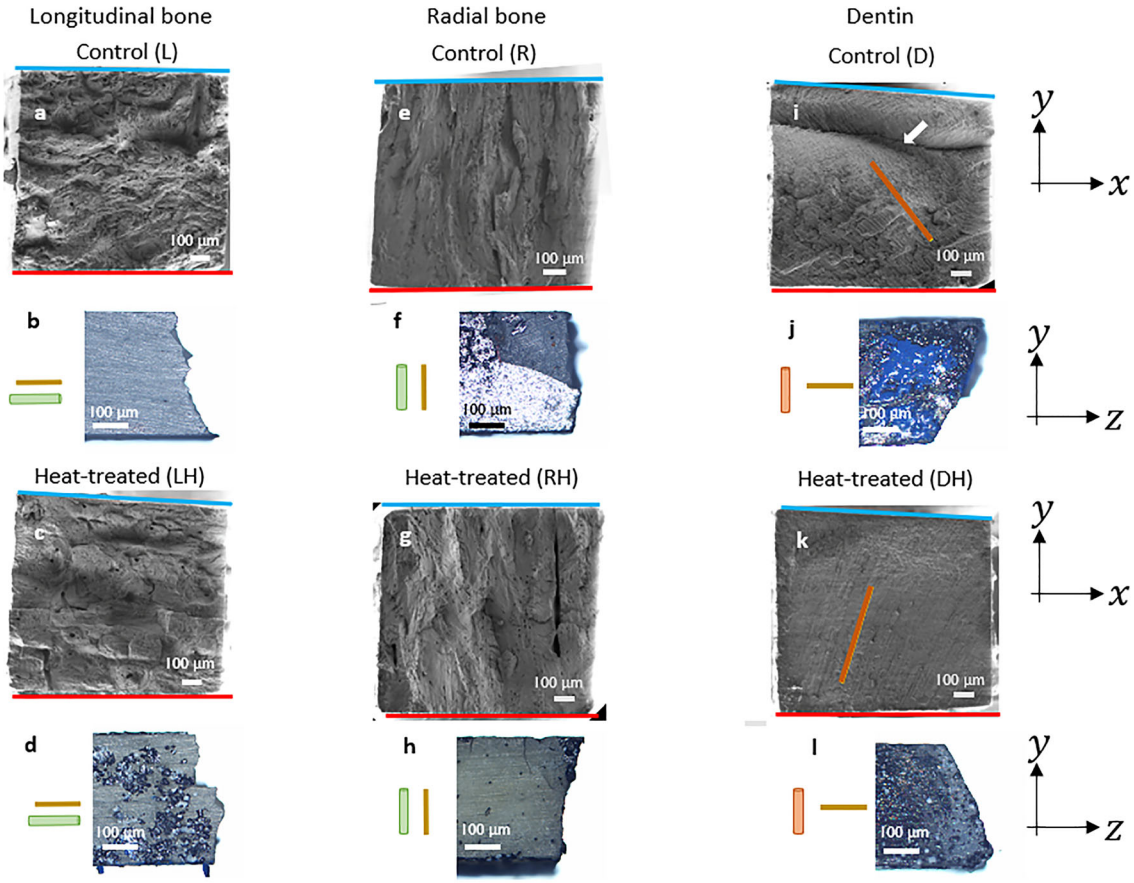

Fig. 4. SEM images of fracture surfaces of longitudinal-oriented cortical bone samples (**a** and **c**), radial-oriented cortical bone samples (**e** and **g**), and human dentin samples (**i** and **k**) paired with optical microscopy side views of the sample (**b**, **d**, **f**, **h**, **j**, **l**). The red lines represent the tension side, and the blue lines represent the compression side of the beam samples. The green lines in (**b**), (**d**), (**f**), and (**h**) indicate the direction of osteons in bones, and the orange lines in (**i**), (**j**), (**k**), and (**l**) the direction of tubules in the dentin. The yellow lines indicate the direction of collagen fibrils. (**b**), (**f**), and (**j**) are lateral views of the crack propagation path in control samples, and (**d**), (**h**), and (**l**) are the same type of views in heat-treated samples. The (*x*, *y*, *z*) coordinates system is direct (Color figure online).

the mineral part that will hinder the participation of collagen fibrils in the homogenized elastic modulus.

For longitudinal bone or dentin samples, we can propose a Voigt configuration[71] for which the Young's modulus of the composite E_L can be assessed:

$$E_L = c_f E_f + c_{HAP} E_{HAP} \tag{2}$$

Here, when E_f decreases, as $E_f << E_{HAP}$, no major change of the global Young's modulus is to be expected. Despite the simplicity of the two proposed rheological models, they are useful to understand the difference of tendencies found in radial and longitudinal bone (or dentin) and to link it with the collagen organisation.

For bone more specifically, collagen denaturation reduces post-yield properties or plasticity of the bone. In bones, as in most materials, plasticity conferred by collagen is a major contributor to intrinsic toughening mechanisms, by dissipating energy and forming "plastic zones" surrounding incipient cracks that further serve to blunt crack tips, thereby reducing the driving force for crack propagation.[72] The reduced plasticity limits energy dissipation and makes the bone more brittle. We also notice that, compared to the bone, the dentin displays more brittle behavior (no post-yield response) for both the heat-treated and untreated samples. As we described in 3, the fracturing of the samples during the bending test was brutal because of the lack of plasticity. We hypothesize that the presence of highly mineralized areas in dentin, e.g., peritubular dentin surrounding tubules and collars surrounding their lateral branches, might be the reason for the lack of plasticity. On the other hand, the fact that there is little or no remodeling in dentin[30] may also contribute to its brittleness compared to bone, considering that a remodeling or repairing procedure would allow the tissue to

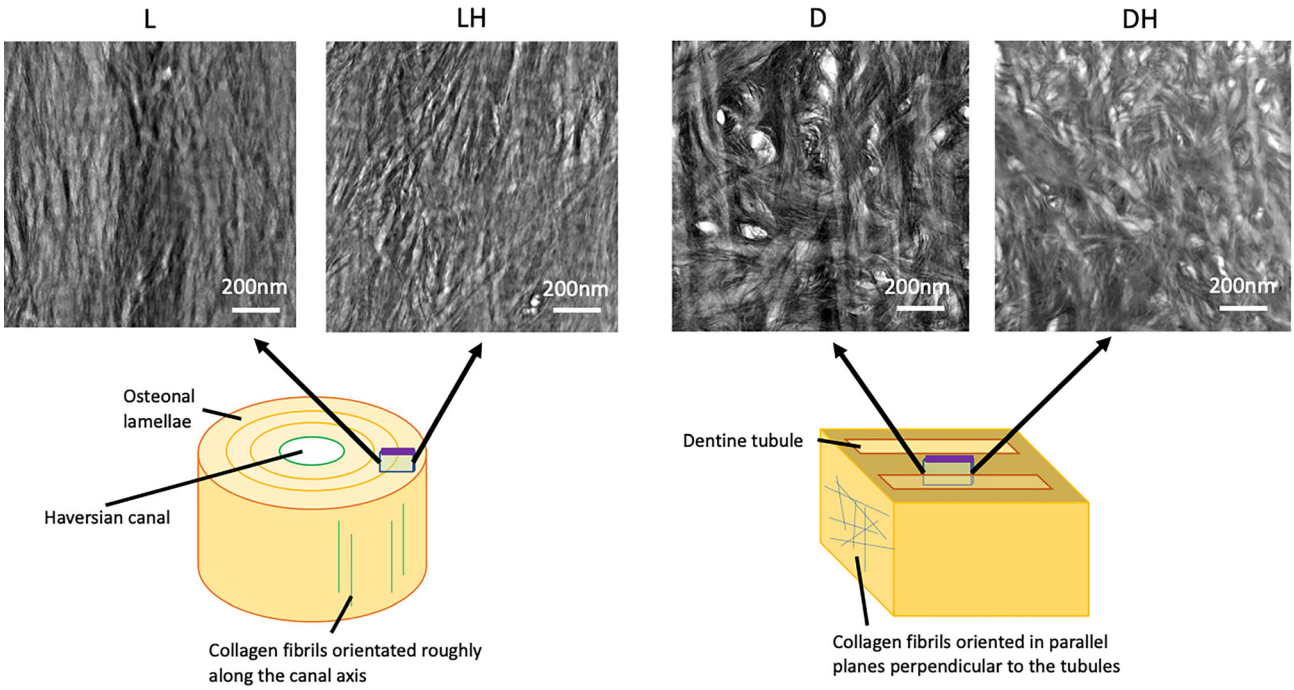

Fig. 5. TEM bright-field image of dentin and longitudinal bone samples (D, DH, L and LH). In D and DH samples the collagen fibrils are crossing the imaged plane whereas in L and LH samples the fibrils are lying within the imaged plane. In L and LH samples the periodic banding appears clearly. No significant differences are observed between control and heat-treated groups.

remove microcracks in highly mineralized areas and recover the resistance to fracture.[73] Exploring deciduous teeth would be an interesting perspective to investigate how younger dentin tissue react to mechanical loading.

Limitations and Perspectives

One limitation of our study is that heat treatment (at 160 °C) does not perfectly replicate the effect of pathological diseases. In addition to unwinding the collagen molecule, it might also affect the mineral-collagen interface and the bonding and cross-linking of the collagen.[74] In addition, pathological diseases, such as osteoporosis, OI, DI, and diabetes, often impact the tissue microstructure and the cells maintaining bone and dentin homeostasis.[7,20,75] This study is a first step towards understanding the different mechanisms causing fragility in these pathologies. In future work, we will be interested in analyzing pathological specimens. On the other hand, in our study we used TEM to observe minerals. It would be be of interest to examine collagen using alternative techniques such as AFM (atomic force microscopy). Finally, bovine cortical bone samples were prepared from the posterior mid-diaphysis of adult femurs. This area presents a Haversian-dominated microstructure with well-formed osteons; however, it might also contain regions of plexiform combined with osteons.[76,77] Therefore, bovine bone microstructure does not perfectly mimic human bone microstructure.

CONCLUSION

This study has confirmed the crucial role of collagen in the microstructural crack propagation and macroscale mechanical and fracture properties of bone and dentin. Our results show that the heat treatment at 160°C leads to a decrease in elastic deformation (and removal of plastic deformation in bone) associated with a lower elastic limit and yield stress in bone and dentin samples. Loss of tissue's ability to deform causes a flatter crack path, which dissipates less energy through the tissue's microstructure. Our results also highlight the importance of the orientation of collagen fibrils and hydroxyapatite crystals on the elastic and plastic properties. Our study provides new insights into the effect of collagen denaturation on the behavior of bone and dentin and contributes to a better understanding of the impact of diseases associated with collagen denaturation such as osteogenesis imperfecta, dentinogenesis imperfect, diabetes, or cancer on these tissues. The results of this study have important implications for the development of new strategies for the diagnosis and treatment of these diseases targeting collagen deficits. Future studies should focus on the relationship between collagen denaturation and loss of resistance in pathological tissues. This will provide a more comprehensive understanding of the role of collagen when compared with other disease-related impairments of tissue structure and cell integrity.

SUPPLEMENTARY INFORMATION

The online version contains supplementary material available at https://doi.org/10.1007/s11837-023-05852-0.

ACKNOWLEDGEMENTS

This work has been supported as part of France 2030 program ANR-11-IDEX-0003.

AUTHOR CONTRIBUTIONS

CA and EV designed research; QW, TR and MV performed research; QW, ST analyzed data; CA, EV, QW, ST wrote the manuscript. All authors have given approval for the final version of the manuscript.

CONFLICT OF INTEREST

On behalf of all authors, the corresponding author states that there is no conflict of interest.

REFERENCES

1. E.A. Zimmermann, R.O. Ritchie, *Adv. Healthc. Mater.* **4**(9), 1287 (2015).
2. R.B. Martin, D.B. Burr, N.A. Sharkey, D.P. Fyhrie, R.B. Martin, D.B. Burr, N.A. Sharkey, D.P. Fyhrie, *Skelet. Tissue Mech.* 355 (2015).
3. A. Carriero, E.A. Zimmermann, A. Paluszny, S.Y. Tang, H. Bale, B. Busse, T. Alliston, G. Kazakia, R.O. Ritchie, S.J. Shefelbine, *J. Bone Miner. Res.* **29**(6), 1392 (2014).
4. M. Biria, F.M. Abbas, S. Mozaffar, R. Ahmadi, *Dental Res. J.* **9**(4) (2012).
5. M.A. Saghiri, B. Rahmani, M. Conte, D. Nath, O.A. Peters, S.M. Morgano, *Eur. Endod. J.* **7**(2), 122 (2022).
6. L.B. Bondarenko, Avicenna J. Med. Biochem. **7**(2), 64 (2019).
7. K.L. Reigle, G. Di Lullo, K.R. Turner, J.A. Last, I. Chervoneva, D.E. Birk, J.L. Funderburgh, E. Elrod, M.W. Germann, C. Surber et al. *J. Cell. Biochem.* **104**(5), 1684 (2008).
8. L.S. Mirigian, E. Makareeva, H. Koistinen, O. Itkonen, T. Sorsa, U.-H. Stenman, T. Salo, S. Leikin, *Arch. Biochem. Biophys.* **535**(2), 111 (2013).
9. M.E. Launey, M.J. Buehler, R.O. Ritchie, *Annu. Rev. Mater. Res.* **40**, 25 (2010).
10. C. Acevedo, V.A. Stadelmann, D.P. Pioletti, T. Alliston, R.O. Ritchie, *Nat. Biomed. Eng.* **2**(2), 62 (2018).
11. C. Acevedo, M. Sylvia, E. Schaible, J.L. Graham, K.L. Stanhope, L.N. Metz, B. Gludovatz, A.V. Schwartz, R.O. Ritchie, T.N. Alliston et al., *J. Bone Miner. Res.* **33**(6), 1066 (2018).
12. V. Imbeni, R. Nalla, C. Bosi, J. Kinney, R. Ritchie, *J. Biomed. Mater. Res. Part A Off. J. Soc. Biomater. Jpn. Soc. Biomater. Aust. Soc. Biomater. Korean Soc. Biomater.* **66**(1), 1 (2003).
13. M. Sieverts, Y. Obata, J.L. Rosenberg, W. Woolley, D.Y. Parkinson, H.S. Barnard, D.M. Pelt, C. Acevedo, *Commun. Mater.* **3**(1), 1 (2022).
14. R.K. Nalla, J.H. Kinney, R.O. Ritchie, *Nat. Mater.* **2**(3), 164 (2003).
15. M. Bath-Balogh, M.J. Fehrenbach, *Illus. Dental Embryol. Histol. Anat. Inst. Resour. Manual* **5**, 160 (2006).
16. X. Feng, *Curr. Chem. Biol.* **3**(2), 189 (2009).
17. J.-Y. Rho, L. Kuhn-Spearing, P. Zioupos, *Med. Eng. Phys.* **20**(2), 92 (1998).
18. F. Baino, *Biomedical, Therapeutic and Clinical Applications of Bioactive Glasses* (2018), pp. 443–466.
19. Y. Wang, T. Azaïs, M. Robin, A. Vallée, C. Catania, P. Legriel, G. Pehau-Arnaudet, F. Babonneau, M.-M. Giraud-Guille, N. Nassif, *Nat. Mater.* **11**(8), 724 (2012).
20. W. Nijhuis, D. Eastwood, J. Allgrove, I. Hvid, H. Weinans, R. Bank, R. Sakkers, *J. Child. Orthop.* **13**(1), 1 (2019).
21. Y. Lin, S. Xu, *J. Microsc.* **241**(3), 291 (2011).
22. B. Yu, A. Pacureanu, C. Olivier, P. Cloetens, F. Peyrin, *Sci. Rep.* **10**(1), 4567 (2020).
23. V. Sansalone, J. Kaiser, S. Naili, T. Lemaire, *Biomech. Model. Mechanobiol.* **12**(3), 533–553 (2013).
24. E. Vennat, W. Wang, R. Genthial, B. David, E. Dursun, A. Gourrier, *Acta Biomater.* **51**, 418–432 (2017).
25. I. Mjör, I. Nordahl, *Arch. Oral Biol.* **41**(5), 401–412 (1996).
26. J. Kinney, J. Pople, G. Marshall, S. Marshall, *Calcif. Tissue Int.* **69**(1), 31 (2001).
27. J. Kim, G. Lee, W.S. Chang, S.H. Ki, J.-C. Park, *J. Bone Metab.* **28**(1), 1 (2021).
28. T. Orvig, *Structural and Chemical Organization of Teeth* (1967), pp. 45–110.
29. K. Kawasaki, A.V. Buchanan, K.M. Weiss, *Cells Tissues Org.* **186**(1), 7 (2007).
30. M. Goldberg, A.B. Kulkarni, M. Young, A. Boskey, *Front. Biosci. (Elite Ed.)* **3**, 711 (2011).
31. S.O. Vital, C. Gaucher, C. Bardet, P. Rowe, A. George, A. Linglart, C. Chaussain, *Bone* **50**(4), 989 (2012).
32. P. Zioupos, J. Currey, A. Hamer, *J. Biomed. Mater. Res. Off. J. Soc. Biomater. Jpn. Soc. Biomater. Aust. Soc. Biomater.* **45**(2), 108 (1999).
33. X. Wang, X. Shen, X. Li, C.M. Agrawal, *Bone* **31**(1), 1 (2002).
34. N.V. Kuznetsova, D.J. McBride Jr., S. Leikin, *J. Mol. Biol.* **331**(1), 191 (2003).
35. X. Wang, X. Li, R. Bank, Agrawal C. *Bone* **4**, 11 (2002).
36. S. Li, E. Demirci, V.V. Silberschmidt, *J. Mech. Behav. Biomed. Mater.* **21**, 109 (2013).
37. A. Mayya, A. Banerjee, R. Rajesh, *Sci. Rep.* **3**(1), 1 (2013).
38. K.E. Stockhausen, M. Qwamizadeh, E.M. Wölfel, H. Hemmatian, I.A. Fiedler, S. Flenner, E. Longo, M. Amling, I. Greving, R.O. Ritchie et al., *ACS Nano* **15**(1), 455 (2021).
39. W. Wagermaier, S. Gupta, H.A. Gourrier, M. Burghammer, P. Roschger, P. Fratzl, *Biointerphases* **1**(1), 1 (2006).
40. H. Ryou, N. Amin, A. Ross, N. Eidelman, D. Wang, E. Romberg, D. Arola, *J. Mater. Sci. Mater. Med.* **22**, 1127 (2011).
41. Y. Li, S.M. Yu, *Collagen: Methods and Protocols* (2019), pp. 135–144.
42. A.H. Lin, J.L. Zitnay, Y. Li, S.M. Yu, J.A. Weiss, *J. Orthop. Res.* **37**(2), 431 (2019).
43. E. Makareeva, E.L. Mertz, N.V. Kuznetsova, M.B. Sutter, A.M. DeRidder, W.A. Cabral, A.M. Barnes, D.J. McBride, J.C. Marini, S. Leikin, *J. Biol. Chem.* **283**(8), 4787 (2008).
44. R.F. Pereira, E.L. Hume, K.W. Halford, D.J. Prockop, *J. Bone Miner. Res.* **10**(12), 1837 (1995).
45. V. Mann, E.E. Hobson, B. Li, T.L. Stewart, S.F. Grant, S.P. Robins, R.M. Aspden, S.H. Ralston et al., *J. Clin. Investig.* **107**(7), 899 (2001).
46. M. Bernad, M. Martinez, M. Escalona, M. Gonzalez, C. Gonzalez, M. Garces, M. Del Campo, E.M. Mola, R. Madero, L. Carreno, *Bone* **30**(1), 223 (2002).
47. A. Mieczkowska, S.A. Mansur, N. Irwin, P.R. Flatt, D. Chappard, G. Mabilleau, *Bone* **76**, 31 (2015).
48. S. Viguet-Carrin, P. Garnero, P. Delmas, *Osteoporos. Int.* **17**(3), 319 (2006).
49. R. Martin, J. Ishida, *J. Biomech.* **22**(5), 419 (1989).
50. P.V. Taufalele, J.A. VanderBurgh, A. Muñoz, M.R. Zanotelli, C.A. Reinhart-King, *PLoS ONE* **14**(5), 0216537 (2019).
51. C.A. Miles, A.J. Bailey, In: *Proceedings of the Indian Academy of Sciences-Chemical Sciences*, vol. 111 (Springer, 1999). pp. 71–80.
52. R. Fraser, T. MacRae, E. Suzuki, *J. Mol. Biol.* **129**(3), 463 (1979).
53. S.P. Robins, A.J. Bailey, *Biochem. J.* **149**(2), 381 (1975).
54. L. Bozec, M. Odlyha, *Biophys. J.* **101**(1), 228 (2011).

55. K. Tai, PhD thesis, Massachusetts Institute of Technology (2007).
56. M.F. Paige, J.K. Rainey, M.C. Goh, *Biophys. J.* **74**(6), 3211 (1998).
57. A. Forlino, W.A. Cabral, A.M. Barnes, J.C. Marini, *Nat. Rev. Endocrinol.* **7**(9), 540 (2011).
58. A. Stylianou, *Materials* **15**(4), 1608 (2022).
59. B. Zeller-Plumhoff, C. Malich, D. Krüger, G. Campbell, B. Wiese, S. Galli, A. Wennerberg, R. Willumeit-Römer, D.F. Wieland, *Acta Biomater.* **101**, 637 (2020).
60. U. Amornkitbamrung, Y. In, Z. Wang, J. Song, S.H. Oh, M.-H. Hong, H. Shin, *ACS Omega* **7**(6), 4821 (2022).
61. Y. In, U. Amornkitbamrung, M.-H. Hong, H. Shin, *ACS Omega* **5**(42), 27204 (2020).
62. R.K. Nalla, J.J. Kruzic, R.O. Ritchie, *Bone* **34**(5), 790 (2004).
63. K.J. Koester, J. Ager, R. Ritchie, *Nat. Mater.* **7**(8), 672 (2008).
64. Y. Liu, A. Li, X. Lin, In: *IOP Conference Series: Earth and Environmental Science*, vol. 512, (IOP Publishing, 2020), p. 012148.
65. N. Iwamoto, N.D. Ruse, *J. Biomed. Mater. Res. Part A Off. J. Soc. Biomater. Jpn. Soc. Biomater. Aust. Soc. Biomater. Korean Soc. Biomater.* **66**(3), 507 (2003).
66. S.T. Rasmussen, R.E. Patchin, D.B. Scott, A.H. Heuer, *J. Dent. Res.* **55**(1), 154 (1976).
67. S. Rasmussen, R. Patchin, *J. Dent. Res.* **63**(12), 1362 (1984).
68. E. Donnelly, D.X. Chen, A.L. Boskey, S.P. Baker, M.C. van der Meulen, *Calcif. Tissue Int.* **87**(5), 450 (2010).
69. E.F. Morgan, M.L. Bouxsein, *Principles Bone Biol.* **1**, 29 (2002).
70. A.H. Burstein, J. Zika, K. Heiple, L. Klein, *JBJS* **57**(7), 956–961 (1975).
71. E. Lucchinetti, *Bone Mechanics Handbook* **2** (2001).
72. E.A. Zimmermann, E. Schaible, H. Bale, H.D. Barth, S.Y. Tang, P. Reichert, B. Busse, T. Alliston, J.W. Ager III., R.O. Ritchie, *Proc. Natl. Acad. Sci.* **108**(35), 14416 (2011).
73. A. Bigham-Sadegh, A. Oryan, *Int. Wound J.* **12**(3), 238 (2015).
74. X. Wang, R.A. Bank, J.M. TeKoppele, C.M. Agrawal, *J. Orthop. Res.* **19**(6), 1021 (2001).
75. K. Beck, V.C. Chan, N. Shenoy, A. Kirkpatrick, J.A. Ramshaw, B. Brodsky, *Proc. Natl. Acad. Sci.* **97**(8), 4273 (2000).
76. S.F. Lipson, J.L. Katz, *J. Biomech.* **17**(4), 231 (1984).
77. A.A. Abdel-Wahab, K. Alam, V.V. Silberschmidt, *J. Mech. Behav. Biomed. Mater.* **4**(5), 807 (2011).